



## Research articles

## Topological magnons in ferromagnetic Kitaev-Heisenberg model on CaVO lattice

Moumita Deb, Asim Kumar Ghosh \*

Department of Physics, Jadavpur University, 188 Raja Subodh Chandra Mallik Road, Kolkata 700032, India

## ARTICLE INFO

## Keywords:

Topological phase

Edge states

Topological phase transition

Thermal hall conductance

Chern numbers

Kitaev-Heisenberg model

## ABSTRACT

A number of topological phases are found to emerge in the ferromagnetic Kitaev-Heisenberg model on CaVO lattice in the presence of Dzyaloshinskii-Moriya interaction. Heisenberg and Kitaev terms have been considered on nearest and next-nearest neighbor bonds in a variety of ways. Both isotropic and anisotropic couplings are taken into account. Topological phases are characterized by Chern numbers for the distinct magnon bands as well as the number of modes for topologically protected gapless magnon edge states. Band structure, dispersion relation along the high-symmetric points of first Brillouin zone, density of states and thermal Hall conductance have been evaluated for every phase. An extensive Phase diagram has been constructed. Topological phase transition in the parameter space is also studied.

## 1. Introduction

Study of topological properties on condensed matter systems hails a new era in theoretical as well as experimental investigations. Chern number ( $\mathcal{C}$ ) is recognized as the topological invariant for the characterization of topological phase of that particular class of topological insulators (TI), where time-reversal symmetry (TRS) is broken [1]. The relation between  $\mathcal{C}$  and number of topologically protected modes of edge state is governed by 'bulk-edge-correspondence' rule [2].  $\mathcal{C}$  of a definite band is determined by integrating the Berry curvature over the first Brillouin zone (BZ). Nontrivial topological phase corresponds to that state where the system exhibits at least a pair of nonzero values of  $\mathcal{C}$ . A variety of many particle interactions are found responsible behind the emergence of non-trivial topological phases. Several kinds of interactions deform the Berry curvatures in so many different ways that they eventually lead to numerous topological phases. Performance of few potential two-spin interactions will be discussed here, those are found crucial to induce non-triviality in magnetic systems.

The first magnetic material who demonstrates non-triviality is  $\text{Lu}_2\text{V}_2\text{O}_7$  [3,4]. The experimental results are explained in terms of a spin-1/2 ferromagnetic (FM) Heisenberg model on a kagomé lattice in the presence of antisymmetric Dzyaloshinskii-Moriya interaction (DMI) [5,6]. Two distinct topological phases characterized by  $\mathcal{C} = (10\bar{1})$  and  $(\bar{1}01)$  appear around the zero DMI strength, where  $\bar{x}$  means  $-x$ . Emergence of those phases can be regarded as the handiwork of DMI term [7,8]. Those states are observed again in another kagomé ferromagnet,

$\text{Cu}[1,3\text{-benzenedicarboxylate (bdc)}]$  [9]. This kind of state is now termed as topological magnon insulating (TMI) phase. In both cases, TMI phase is observed in the presence of an external magnetic field which acts as a TRS breaking component in the system.

In another development, FM Heisenberg models consisting of both nearest-neighbor (NN) Kitaev [10] and symmetric spin-anisotropic interactions (SAI) are found to exhibit TMI phases on the honeycomb lattice in the presence of magnetic field. This two-band system hosts the TMI phase with  $\mathcal{C} = (1\bar{1})$ , when both the two-spin interacting terms are present [11]. This model is extended beyond NN interactions by including third-neighbor Kitaev and SAI terms which is found to host multiple novel TMI phases with higher Chern numbers [12]. DMI term fails to induce non-triviality in this honeycomb model. It is worth mentioning that multiple TMI phases are found in the triplet six-spin plaquette excitations of the antiferromagnetic (AFM) Heisenberg model on the honeycomb lattice without the DMI terms [13]. Thus search for new combinations of two-spin terms continues those are capable to induce non-triviality in other lattice geometries.

In this article, emergence of multiple TMI phases will be reported in a four-band FM Heisenberg model formulated on a CaVO lattice which includes both NN and next-nearest-neighbor (NNN) Heisenberg and Kitaev terms along with NNN DMI term. NN DMI term has no effect on the topological phases, while presence of NNN DMI turns out to be indispensable for the emergence of topological phases. Again, DMI only on the NN bonds alone fails to drive the system into the topologically nontrivial regime. Remarkably, SAI is found to play in this system while

\* Corresponding author.

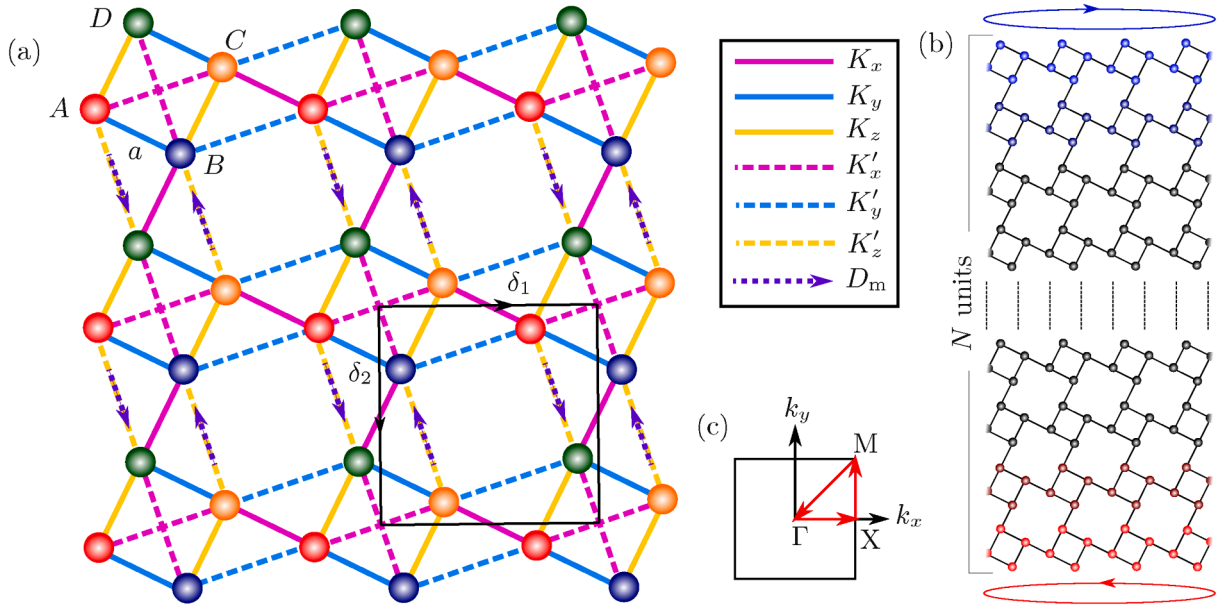


**Fig. 1.** (a) Geometrical view of the model with NN and NNN interactions on the CaVO lattice. Opposite arrowheads indicate the opposite directions of DMI terms. (b) Geometry of the lattice used for edge state calculation, upper and lower edges are drawn in blue and red colors, respectively. (c) The first Brillouin zone showing the high-symmetry points,  $\Gamma$ , M and X.

the TRS breaking magnetic field is taken into account for obvious reason. Emergence of photo-induced multiple topological phases is reported before in a tight-binding model on CaVO lattice [14]. Existence of multiple Dirac nodal-lines in AFM magnons and triplet excitations are noted for a Heisenberg model on this lattice [15,16].

CaVO lattice has been brought to light before in the context of AFM compound,  $\text{CaV}_4\text{O}_9$  [17]. The spin-1/2  $\text{V}^{4+}$  ions in this frustrated system constitute CaVO lattice structure [18]. Coordination number for both honeycomb and CaVO lattices is three while their symmetries are different. For example, honeycomb (CaVO) lattice has the six (four)-fold rotational symmetry,  $C_6$  ( $C_4$ ). Primitive cell contains two and four lattice points for honeycomb and CaVO lattices, respectively. FM Kitaev models with anisotropic NN bond strengths based on those non-Bravais lattices have been solved exactly in terms of Majorana fermions [10,19]. The gapless phases for both the lattices become topologically nontrivial as soon as the magnetic field is switched on. The topological phase of both honeycomb and CaVO Kitaev models is unique in a sense that the resulting two-band system carries  $\mathcal{C} = (1\bar{1})$  in the Majorana fermion representation. In contrast, no topological phase based on the bosonic magnon excitation emerges in the NN Kitav models on honeycomb and CaVO lattices in the presence of magnetic field.

Hamiltonian is formulated in Section 2. The linear spin-wave theory (LSWT) is developed here. Numerical evaluation of  $\mathcal{C}$ , edge states and thermal Hall conductance (THC) have been described in Section 3. THC experiences sudden jump in the vicinity of phase transition points. The system exhibits seventeen distinct topological phases in total. Half dozen of them appears when isotropic Kitaev interaction is assumed while a dozen appears for anisotropic case. Only one phase is found common in both the cases. Topological phase diagrams have been produced in various forms. A discussion based on those results is available in Section 4.

## 2. Kitaev-Heisenberg model with Dzyaloshinskii-Moriya interactions on the CaVO lattice

In order to develop the spin wave theory, a general form of spin Hamiltonian is considered which contains three specific two-spin interacting terms, say, Kitaev, Heisenberg and DMI in the presence of an external magnetic field. Both Kitaev and Heisenberg terms are pre-

sent on the NN and NNN bonds of the CaVO lattice while DMI is present on a pair of opposite NNN bonds within the octagon plaquette. The Hamiltonian (Eq. 1) is written as

$$\mathcal{H} = J \sum_{\langle ij \rangle} \mathbf{S}_i \cdot \mathbf{S}_j + 2 \sum_{\langle\langle ij \rangle\rangle} K_\gamma S_i^\gamma S_j^\gamma + J' \sum_{\langle\langle ij \rangle\rangle} \mathbf{S}_i \cdot \mathbf{S}_j + 2 \sum_{\langle\langle ij \rangle\rangle} K'_\gamma S_i^\gamma S_j^\gamma + \mathbf{D}_m \cdot \sum_{\langle\langle ij \rangle\rangle} \mathbf{S}_i \times \mathbf{S}_j - \mathbf{h} \cdot \sum_i \mathbf{S}_i. \quad (1)$$

Here,  $J$  ( $J'$ ) and  $K_\gamma$  ( $K'_\gamma$ ) are the Heisenberg and Kitaev interaction strengths respectively for the NN (NNN) bonds. DMI strength is denoted by  $D_m$ . Every site of the CaVO lattice is connected with the others by three NN bonds as well as three NNN bonds. In order to assign the Kitaev interactions, three different components are represented by  $\gamma = x, y, z$ , both for NN and NNN bonds.  $\mathbf{h} = g\mu_B \mathbf{H}$ , where  $H$  is the strength of magnetic field which is acting along the  $+\hat{z}$  direction.  $S_i^\alpha$  is the  $\alpha$ -th component of spin operator,  $S_i$ , at the  $i$ -th site, where  $\alpha = x, y, z$ . Summations over NN and NNN bonds are shown by the indices  $\langle \cdot \rangle$  and  $\langle\langle \cdot \rangle\rangle$ , respectively. Periodic boundary condition (PBC) is assumed along both  $x$  and  $y$  directions. Values of  $J$  and  $J'$  are always negative when they are nonzero. Both positive and negative values of  $K$  and  $K'$  are considered, but magnitudes of  $J$  and  $J'$  are always greater than those of  $K$  and  $K'$  in the isotropic case to ensure the FM ground state.  $J$  and  $J'$  are assumed zero in the anisotropic case, without any loss of generality.

Schematic view of this spin model is given in Fig. 1 (a), where NN (NNN) bonds are indicated by solid (dashed) lines.  $\delta_1$  and  $\delta_2$  are the two primitive vectors to constitute the primitive cell (a square of arm length  $\sqrt{5}a$ ) of the CaVO lattice. The primitive cell represented by the square encloses four nonequivalent sites A, B, C and D, shown by red, blue, yellow and green spheres, respectively. Obviously, the CaVO lattice can be decomposed in terms of four interpenetrating square lattices made of each for four sites A, B, C and D, separately. Alternately, the resulting lattice can be thought of as a specific structure of 1/5-depleted square lattice which preserves the fourfold rotational symmetry,  $\mathcal{C}_4$ , of the square lattice itself.

No topological phase will appear in this model if DMI is absent. Additionally, the direction of  $\mathbf{D}_m$  as well as the combination of bonds on which DMI is acting are very crucial for the emergence of topological phases. For example, DMI on every NN and NNN bond within the square

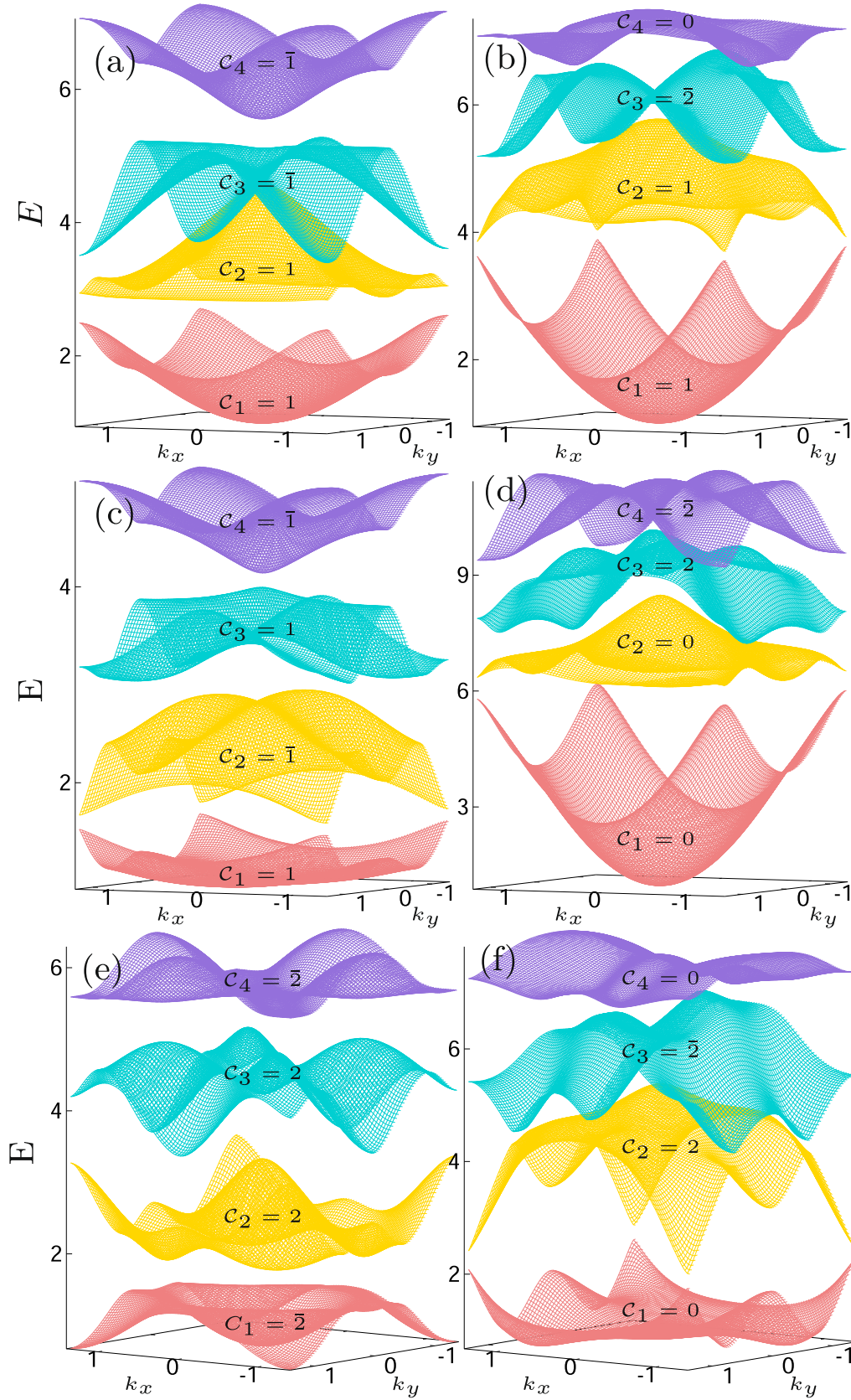


**Fig. 2.** The magnon bands. a)  $J = -1, D_m = 0.5$  for  $\mathcal{C} = (11\bar{1}\bar{1})$ , (b)  $J = -1, K' = -0.5, D_m = 0.5$  for  $\mathcal{C} = (11\bar{2}0)$ , (c)  $J = -1, K = 0.5, D_m = 0.5$  for  $\mathcal{C} = (1\bar{1}1\bar{1})$ , (d)  $J = -1, J' = -0.5, K' = -1, D_m = 1$  for  $\mathcal{C} = (002\bar{2})$ , (e)  $J' = -0.5, K' = -0.5, D_m = 1$  for  $\mathcal{C} = (\bar{2}22\bar{2})$ , and (f)  $J = -1, K = 0.5, K' = -1, D_m = 1$  for  $\mathcal{C} = (02\bar{2}0)$ , with  $h = 1$ . Parameters of non-zero values are indicated here.

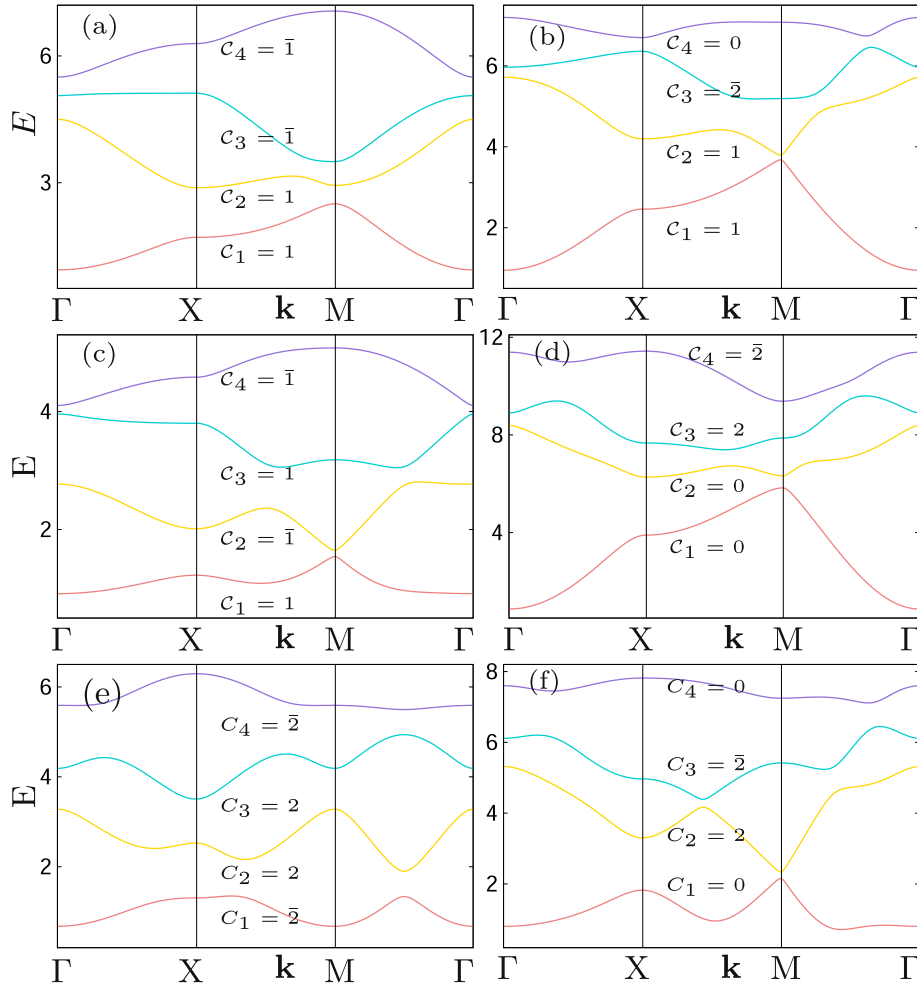


Fig. 3. Dispersion relation along the high-symmetry points of Brillouin zone. Values of the parameters are the same as Fig. 2 for the respective plots.

plaquette does not lead to non-trivial topological phase by any means. It is found that only two specific combinations comprising of two pairs of opposite NNN bonds within the octagon plaquette where the directions of  $\mathbf{D}_m$  are also opposite to each other could lead to the nontriviality. One of such combination is shown in Fig. 1 (a), in which DMI is acting over  $AD$  and  $BC$  bonds but opposite in directions. Opposite arrowhead over  $AD$  and  $BC$  bonds imply the directions of  $\mathbf{D}_m$ , which are  $\pm\hat{z}$ , for the respective bonds. DMI over  $AB$  and  $CD$  bonds may form another potential combination if the directions of that are chosen opposite to each other. However, the later choice is not assumed here, since it fails to exhibit additional topological phases by any means.

The magnon dispersion relations based on the exact FM ground state are obtained by converting the spin operators in terms of bosonic creation ( $b^\dagger$ ) and annihilation ( $b$ ) operators via the Holstein-Primakoff transformation,

$$S_j^z = S - b_j^\dagger b_j, \quad S_j^+ \simeq \sqrt{2S} b_j, \quad S_j^- \simeq \sqrt{2S} b_j^\dagger. \quad (2)$$

Hamiltonian (Eq. 1) has been expressed in the momentum space by Fourier-transforming the operators in that space,  $b_j = \frac{1}{\sqrt{N}} \sum_{\mathbf{k}} b_{\mathbf{k}} e^{i\mathbf{k} \cdot \mathbf{R}_j}$ , where  $N$  is the total number of primitive cells. Thus, the Hamiltonian with respect to the ground state energy,  $E_G = 2NS^2[3(J + J') + 2(K_z + K_z')] - 4NS$ , is

$$\mathcal{H} = \frac{S}{2} \sum_{\mathbf{k}} \Psi_{\mathbf{k}}^\dagger \mathcal{X}_{\mathbf{k}} \Psi_{\mathbf{k}}, \quad (3)$$

where,  $\Psi_{\mathbf{k}}^\dagger = [b_{A,\mathbf{k}}^\dagger, b_{B,\mathbf{k}}^\dagger, b_{C,\mathbf{k}}^\dagger, b_{D,\mathbf{k}}^\dagger, b_{A,-\mathbf{k}}, b_{B,-\mathbf{k}}, b_{C,-\mathbf{k}}, b_{D,-\mathbf{k}}]$ . Now,  $b_A^\dagger, b_B^\dagger, b_C^\dagger$  and  $b_D^\dagger$  are the bosonic creation operators on the sublattices  $A, B, C$  and  $D$ , respectively. Terms containing product of four bosonic operators have been neglected since they invoke inter-magnon interactions.  $\mathcal{X}_{\mathbf{k}}$  is a  $8 \times 8$  matrix, which can be expressed in terms of two different  $4 \times 4$  matrices,  $X_{\mathbf{k}}$  and  $Y_{\mathbf{k}}$  as

$$\mathcal{X}_{\mathbf{k}} = \begin{bmatrix} X_{\mathbf{k}} & Y_{\mathbf{k}} \\ Y_{\mathbf{k}}^\dagger & X_{-\mathbf{k}}^T \end{bmatrix}, \quad (4)$$

where, both  $X_{\mathbf{k}}$  and  $Y_{\mathbf{k}}$  are Hermitian.

$$X_{\mathbf{k}} = \begin{bmatrix} a_0 & a_{1,\mathbf{k}} & a_{2,\mathbf{k}} & a_{3,\mathbf{k}} \\ a_{1,\mathbf{k}}^* & a_0 & a_{4,\mathbf{k}} & a_{5,\mathbf{k}} \\ a_{2,\mathbf{k}}^* & a_{4,\mathbf{k}}^* & a_0 & a_{6,\mathbf{k}} \\ a_{3,\mathbf{k}}^* & a_{5,\mathbf{k}}^* & a_{6,\mathbf{k}}^* & a_0 \end{bmatrix}, \quad Y_{\mathbf{k}} = \begin{bmatrix} 0 & b_{1,\mathbf{k}} & b_{2,\mathbf{k}} & b_{3,\mathbf{k}} \\ b_{1,-\mathbf{k}} & 0 & b_{4,\mathbf{k}} & b_{5,\mathbf{k}} \\ b_{2,-\mathbf{k}} & b_{4,-\mathbf{k}} & 0 & b_{6,\mathbf{k}} \\ b_{3,-\mathbf{k}} & b_{5,-\mathbf{k}} & b_{6,-\mathbf{k}} & 0 \end{bmatrix}. \quad (5)$$

Considering the spin polarization along the  $+z$  direction components of



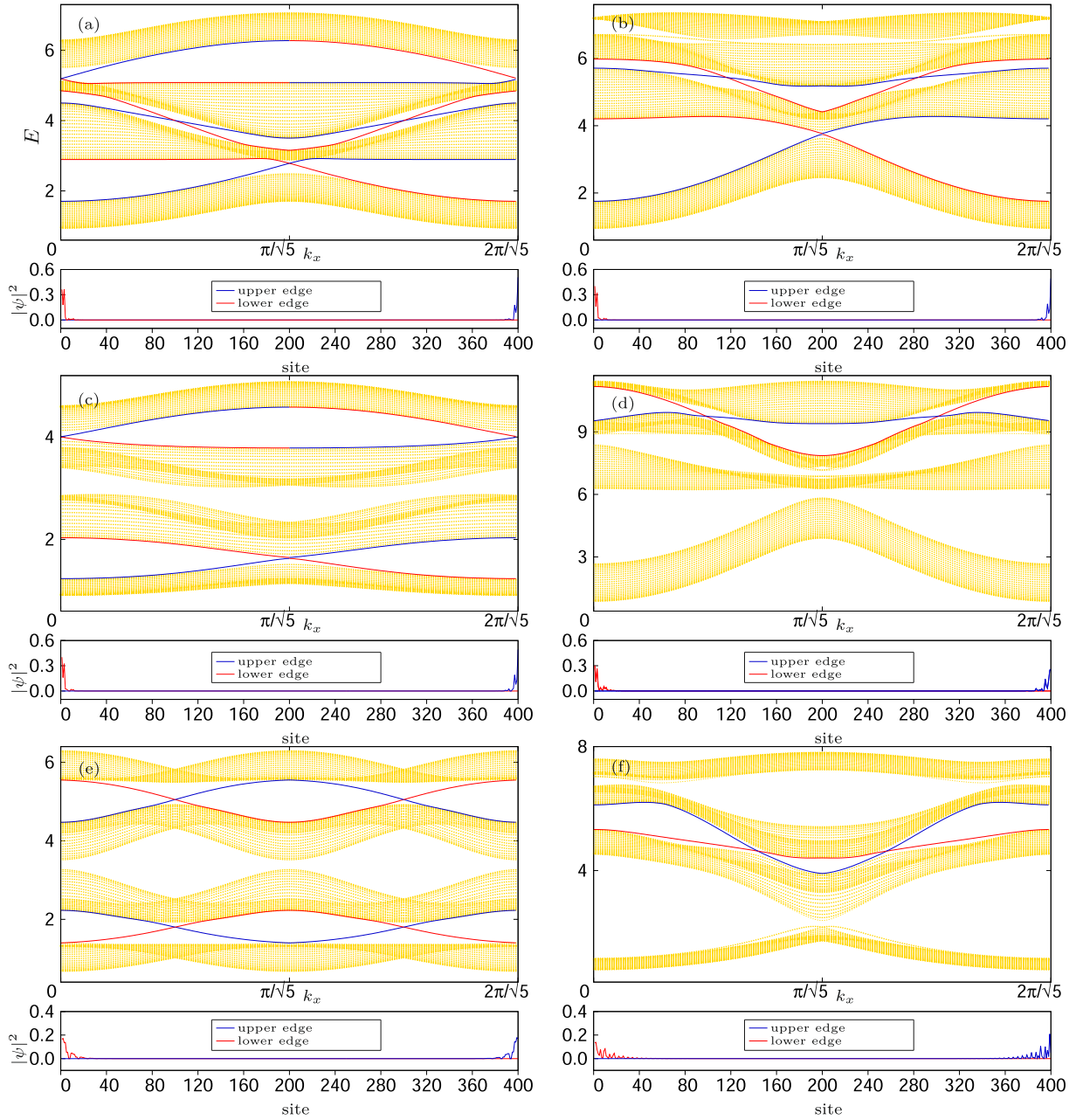


**Fig. 4.** Magnon dispersions of bulk-edge states in the one-dimensional BZ. Upper and lower edge modes are drawn in blue and red lines, respectively, while bulk modes are in golden points. The lower panel indicates variation of probability density of both edge modes with respect to site number for a fixed  $k_x$ . Values of the parameters are: a)  $J = -1, D_m = 0.5$  for  $\ell = (1111)$ , (b)  $J = -1, K' = -0.5, D_m = 0.5$  for  $\ell = (1120)$ , (c)  $J = -1, K = 0.5, D_m = 0.5$  for  $\ell = (1111)$ , (d)  $J = -1, J' = -0.5, K' = -1, D_m = 1$  for  $\ell = (0022)$ , (e)  $J' = -0.5, K' = -0.5, D_m = 1$  for  $\ell = (2222)$ , and (f)  $J = -1, K = 0.5, K' = -1, D_m = 1$  for  $\ell = (0220)$ , with  $h = 1$ . Parameters with only nonzero values are mentioned here.

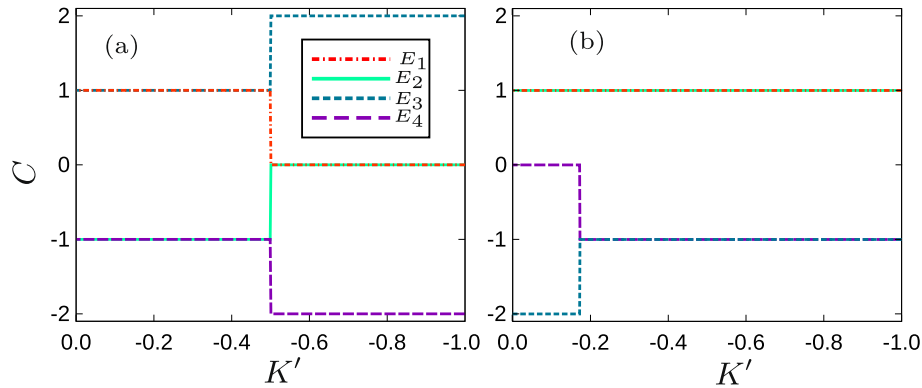


**Fig. 5.** Variation of Chern numbers with  $K'$  for (a)  $K = -0.5, J' = -1$ , and (b)  $K = 1, J' = -0.5$ . For each case  $J = -1, D_m = 1$  and  $h = 1$ .

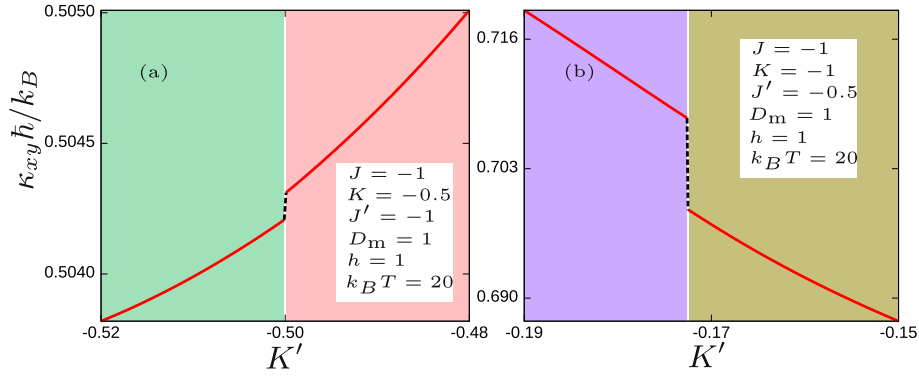


Fig. 6. Variation of  $\kappa_{xy}\hbar/k_B$  in the parameter space when  $T$  is fixed. Different regions are identified with distinct colors.

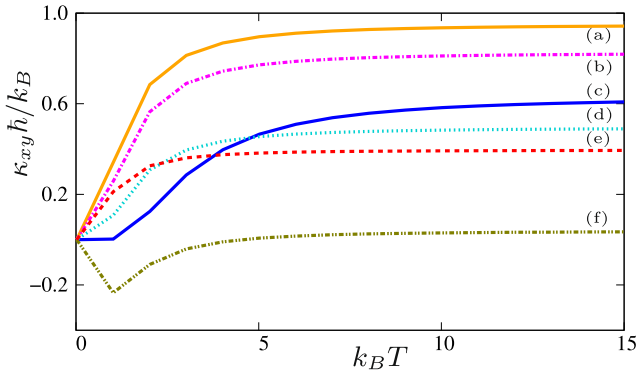


Fig. 7. Variation of  $\kappa_{xy}(T)$  with  $T$  for a)  $J = -1, D_m = 0.5$  for  $\mathcal{C} = (11\bar{1}\bar{1})$ , (b)  $J = -1, K' = -0.5, D_m = 0.5$  for  $\mathcal{C} = (11\bar{2}0)$ , (c)  $J = -1, K = 0.5, D_m = 0.5$  for  $\mathcal{C} = (1\bar{1}1\bar{1})$ , (d)  $J = -1, J' = -0.5, K' = -1, D_m = 1$  for  $\mathcal{C} = (002\bar{2})$ , (e)  $J' = -0.5, K' = -0.5, D_m = 1$  for  $\mathcal{C} = (\bar{2}22\bar{2})$ , and (f)  $J = -1, K = 0.5, K' = -1, D_m = 1$  for  $\mathcal{C} = (02\bar{2}0)$ , with  $h = 1$ . No value is assigned to those parameters when they are zero.

$X_{\mathbf{k}}$  and  $Y_{\mathbf{k}}$  are obtained below.

$$\begin{aligned}
 a_0 &= -3J - 2K_z - 3J' - 2K'_z + h/S, \\
 a_{1,\mathbf{k}} &= (J + K_y) + (J' + K'_y)e^{ik\delta_1}, \\
 a_{2,\mathbf{k}} &= (J + K_x)e^{ik\delta_1} + (J' + K'_x), \\
 a_{3,\mathbf{k}} &= J + J'e^{-ik\delta_2} - iD_me^{-ik\delta_2}, \\
 a_{4,\mathbf{k}} &= J + J'e^{-ik\delta_2} + iD_me^{-ik\delta_2}, \\
 a_{5,\mathbf{k}} &= (J + K_x)e^{-ik\delta_2} + (J' + K'_x), \\
 a_{6,\mathbf{k}} &= (J + K_y) + (J' + K'_y)e^{-ik\delta_1}, \\
 b_{1,\mathbf{k}} &= -K_y - K'_ye^{ik\delta_1}, \\
 b_{2,\mathbf{k}} &= K_xe^{ik\delta_1} + K'_x, \\
 b_{3,\mathbf{k}} &= b_{4,\mathbf{k}} = 0, \\
 b_{5,\mathbf{k}} &= K_xe^{-ik\delta_2} + K'_x, \\
 b_{6,\mathbf{k}} &= -K_y - K'_ye^{-ik\delta_1}, \text{ with,} \\
 \delta_1 &= a\sqrt{5}\hat{i}, \delta_2 = a\sqrt{5}\hat{j}.
 \end{aligned}$$

Here,  $a$  is the length of NN bond which is assumed to be unity. Following the Bogoliubov diagonalization method applicable for the bosonic operators, the non-Hermitian matrix,  $I_{\mathbf{B}}\mathcal{H}_{\mathbf{k}}$  has been diagonalized, instead of  $\mathcal{H}_{\mathbf{k}}$ , in order to obtain the eigenenergies and eigenmodes where  $I_{\mathbf{B}} = \text{diag}[1, 1, 1, 1, -1, -1, -1, -1]$ . Four positive eigenenergies of  $I_{\mathbf{B}}\mathcal{H}_{\mathbf{k}}$  are thus treated as the magnon excitation energies of the system. Accuracy of the results increases with the value of  $S$ . Topological phases have been obtained in the regime where the real eigenenergies are available. Eigenenergies thus constitute the four-band magnon dispersion relations. Band structure varies with the value of magnetic field in such a

fashion that no alteration of the topological phases is found.

### 3. Chern number, edge states, thermal Hall conductance and the topological phases

In order to characterize topological phases of this four-bands system, the Chern number for each distinct magnon band is obtained, when there remains a definite gap between adjacent bands. Chern number for the  $i$ -th band,  $\mathcal{C}_i$ , is obtained by integrating the Berry curvature of that band,  $\mathcal{F}_i(\mathbf{k})$  over the BZ.

$$\mathcal{C}_i = \frac{1}{2\pi} \int_{\text{BZ}} \mathcal{F}_i(\mathbf{k}) d^2\mathbf{k}, \quad (6)$$

where,  $\mathcal{F}_i(\mathbf{k})$  is expressed in terms of the corresponding Berry connection,  $\mathcal{A}_\mu^i(\mathbf{k}) = \langle \psi_i(\mathbf{k}) | \partial_{k_\mu} | \psi_i(\mathbf{k}) \rangle$  as  $\mathcal{F}_i(\mathbf{k}) = \partial_{k_x} \mathcal{A}_y^i(\mathbf{k}) - \partial_{k_y} \mathcal{A}_x^i(\mathbf{k})$ , and  $|\psi_i(\mathbf{k})\rangle$  is the eigenvector of the  $i$ -th magnon band.  $\mathcal{C}_i$  has been evaluated numerically [20].

According to the ‘bulk-edge-correspondence’ rule the presence of nonzero value of  $\mathcal{C}$  implies the existence of edge states. Edge state corresponds to the surface property of the system. To calculate the bulk-edge energy spectrum a pair of edges parallel to the  $x$ -axis is created here by breaking the PBC along the  $y$ -axis. As a result, a strip of CaVO lattice is constructed which has  $N$  primitive cells along the  $\hat{y}$  and infinitely long towards the  $\hat{x}$ . The corresponding lattice structure is shown in Fig. 1(b). Fourier transform of the bosonic operators is taken only along the  $x$  direction and  $4N \times 4N$  Hamiltonian has been obtained.

THC,  $\kappa_{xy}$ , of the system can be expressed in terms of  $\mathcal{F}(\mathbf{k})$  for the system as [23,24],

$$\kappa_{xy}(T) = -\frac{k_B^2 T}{4\pi^2 \hbar} \sum_i \int_{\text{BZ}} c(\rho_i(\mathbf{k})) \mathcal{F}_i(\mathbf{k}) d^2\mathbf{k}. \quad (7)$$

Here  $T$  is the temperature,  $k_B$  is the Boltzmann constant and  $\hbar$  is the reduced Planck’s constant.  $c(x) = (1+x) \left( \ln \frac{1+x}{x} \right)^2 - (\ln x)^2 - 2\text{Li}_2(-x)$ , where  $\text{Li}_2(z) = -\int_0^z \frac{\ln(1-u)}{u} du$  and  $\rho_i(\mathbf{k})$  is the Bose-Einstein distribution, i.e.,  $\rho_i(\mathbf{k}) = 1/(e^{E_i/k_B T} - 1)$ . Like all thermodynamic quantities,  $\kappa_{xy}(T)$  also gets saturated at high temperatures. As  $\kappa_{xy}(T)$  directly depends on the Berry curvature so it behaves differently in different topological phases. As a result,  $\kappa_{xy}$  suffers sudden change in its value at the phase transition points.

In this study, isotropic Heisenberg interaction on the NN and NNN bonds is assumed, while both isotropic and anisotropic Kitaev couplings are taken into account. Anisotropic XXZ Heisenberg interaction on the NN and NNN bonds is not considered here because of the following reason. Total Hamiltonian containing isotropic Heisenberg and DMI terms can be mapped on to the anisotropic XXZ Heisenberg Hamiltonian via a canonical transformation of the spin operators, which is valid for

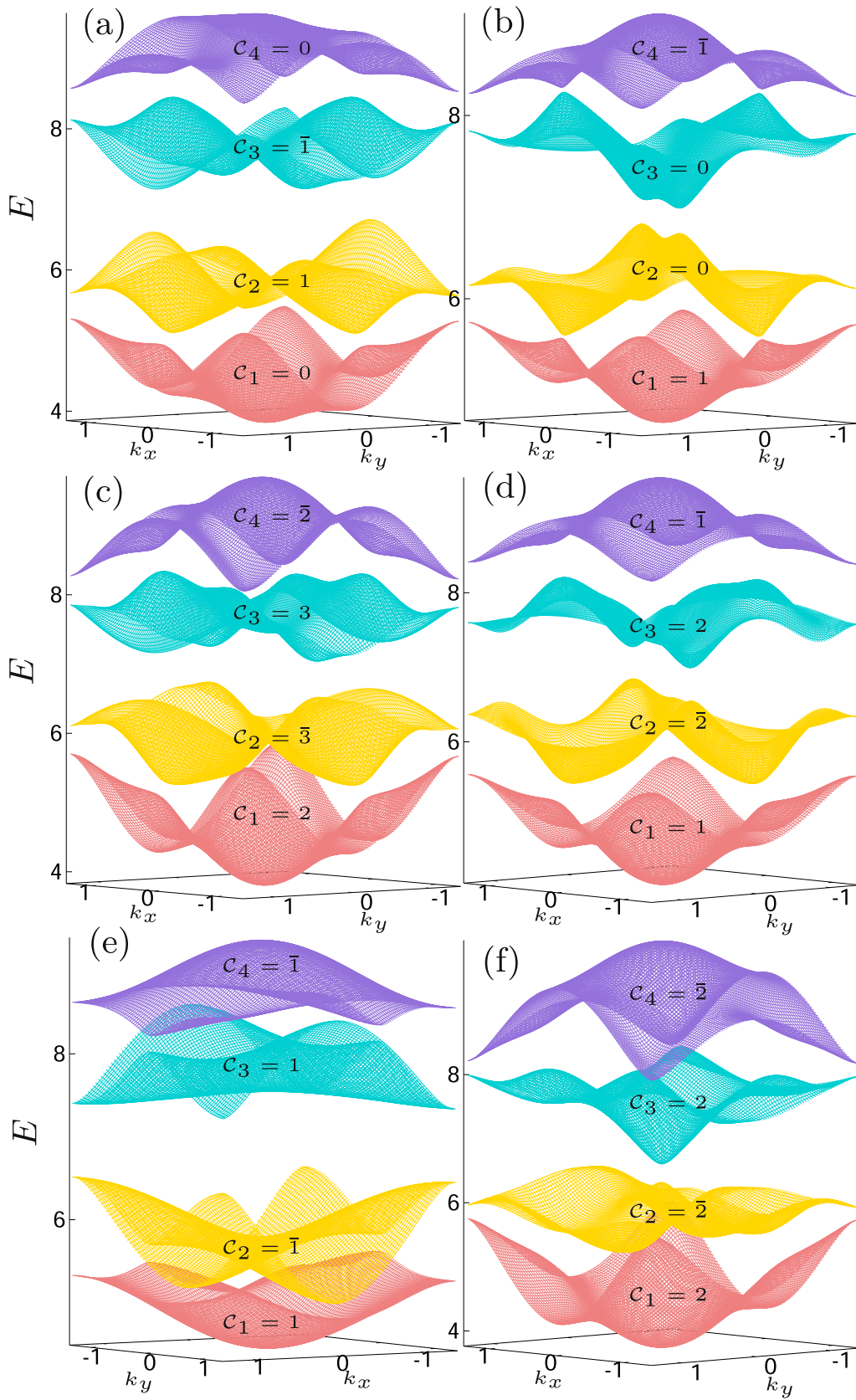


**Fig. 8.** The magnon bands. Values of the parameters are: (a)  $K_x = -0.8, K_y = -0.6, K'_x = -1, K'_y = 0.4$  for  $\mathcal{C} = (01\bar{1}0)$ , (b)  $K_x = -0.7, K_y = -0.2, K'_x = -0.5, K'_y = 0.1$  for  $\mathcal{C} = (100\bar{1})$ , (c)  $K_x = -0.8, K'_x = -1, K'_y = -0.4$  for  $\mathcal{C} = (2\bar{3}3\bar{2})$ , (d)  $K_x = -1, K_y = -0.1, K'_x = -0.6, K'_y = -0.3$  for  $\mathcal{C} = (1\bar{2}2\bar{1})$ , (e)  $K_x = -0.7, K_y = -0.8, K'_x = -0.1, K'_y = -0.5$  for  $\mathcal{C} = (1\bar{1}1\bar{1})$ , and (f)  $K_x = -0.7, K_y = -0.4, K'_x = -0.8, K'_y = -0.9$  for  $\mathcal{C} = (2\bar{2}2\bar{2})$ , with  $K_z = -2, K'_z = -1, D_m = 1, h = 1$ . No value is assigned to those parameters when they are zero.

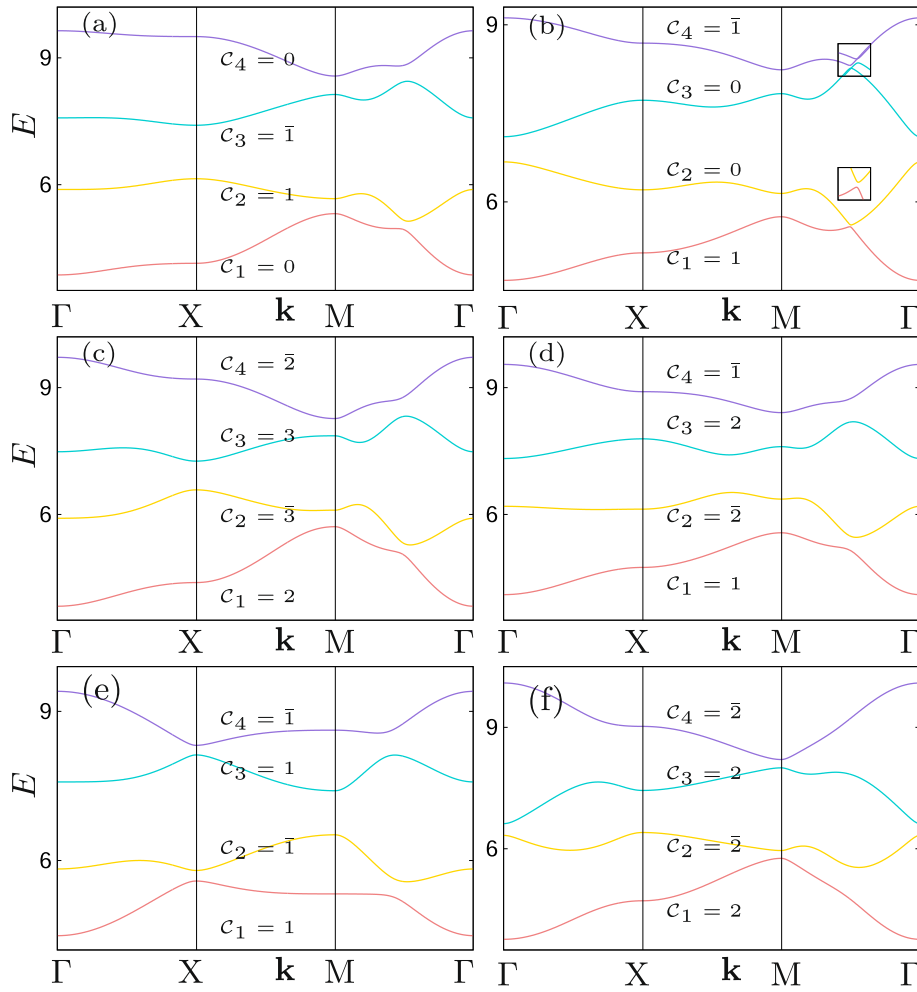


Fig. 9. Dispersion relation along the high-symmetry points of Brillouin zone. Values of the parameters are the same as Fig. 8 for the respective plots.

any values of  $S$  [21]. It is true even for arbitrary directions of  $D_m$  over different bonds as long as they are parallel or antiparallel to each other [22]. Which means that effect of DMI term on the Heisenberg model can be studied in terms of a suitable XXZ Heisenberg Hamiltonian where the value of anisotropic parameter depends on the values of exchange and DMI strengths. So, in other words, inclusion of anisotropic Heisenberg interaction could not lead to the emergence of new topological phases anymore.

For example, the same set of two distinct topological phases with  $\mathcal{C} = (10\bar{1})$  and  $(\bar{1}01)$ , appear in two previously studied models where isotropic and anisotropic XXZ Heisenberg Hamiltonians are formulated on kagomé lattice in the presence of DMI [7,8]. A closer scrutiny on those two models reveals that only the diagonal terms of those Hamiltonian matrices ( $H_{ij}$ ) are different, where the values of  $\mathcal{C}$ s are insensitive to them. Off-diagonal matrix elements satisfy the relation,  $H_{ij}(-D_m) = H_{ij}^*(D_m)$ , which on the other hand corresponds to the band inversion about  $D_m = 0$ , in this particular case [7]. And as a result,  $\mathcal{C}$ s of the two topological phases exhibit mirror symmetry around the middle band.

Here, the system hosts seventeen distinct topological phases in total. Six are found for the isotropic Kitaev coupling but twelve for the anisotropic case. All of them are described in the following two subsections. One phase is found common in both the cases. Every topological phase is described by band structure, dispersion relation along the high-symmetric points of first Brillouin zone, density of states (DOS) and thermal Hall conductance. Value of  $\mathcal{C}$  for each distinct band has been evaluated in association with the bulk-edge energy spectrum for the Hamiltonian formulated on the strip of CaVO lattice of finite length

along y-axis.

### 3.1. Isotropic Kitaev coupling

In this case, the same value of Kitaev interaction along three different links of the lattice is considered, which means,  $K_\gamma = K$  and  $K'_\gamma = K'$ . Similar model on the two-band honeycomb lattice exhibits multiple TMI phase with higher values of  $\mathcal{C}$ s, when third neighbor interactions are invoked [12]. In this study, isotropic Kitaev model on the CaVO lattice is found to exhibit six topological phases. Bulk energy dispersion with specific values of  $\mathcal{C}$  have been plotted in Fig. 2 for different TMI phases. Dispersion relations along the high-symmetry points of BZ are shown in Fig. 3. Dispersions of bulk-edge states in the one-dimensional BZ have been shown in Fig. 4. Edge state dispersion branches for upper (blue) and lower (red) edges are indicated in different colors.

TMI phases as well as band gaps appear as soon as NNN DMI is switched on. Let us now describe the TMI phases shown in Fig. 2. Two distinct topological phases appear when all other NNN bond strengths are zero. These are  $\mathcal{C} = (11\bar{1}\bar{1})$  and  $\mathcal{C} = (\bar{1}\bar{1}1\bar{1})$ , as shown in Fig. 2 (a) and (c), respectively, when  $J = -1, D_m = 0.5$  and  $J = -1, K = 0.5, D_m = 0.5$ , in two respective cases.  $\mathcal{C}$ s are expressed following the ascending order of energy value in every case. The remaining four phases appear in the presence of other NNN bond strengths. Among them  $\mathcal{C} = (2\bar{2}2\bar{2})$  appears when all the NN interactions are absent. Therefore, TMIs with  $\mathcal{C} = (11\bar{2}0)$ ,  $\mathcal{C} = (002\bar{2})$  and  $\mathcal{C} = (02\bar{2}0)$  emerges when both NN and NNN terms are present. However, appearance of those phases is by no means fixed for those particular values of the parameters. Those phases



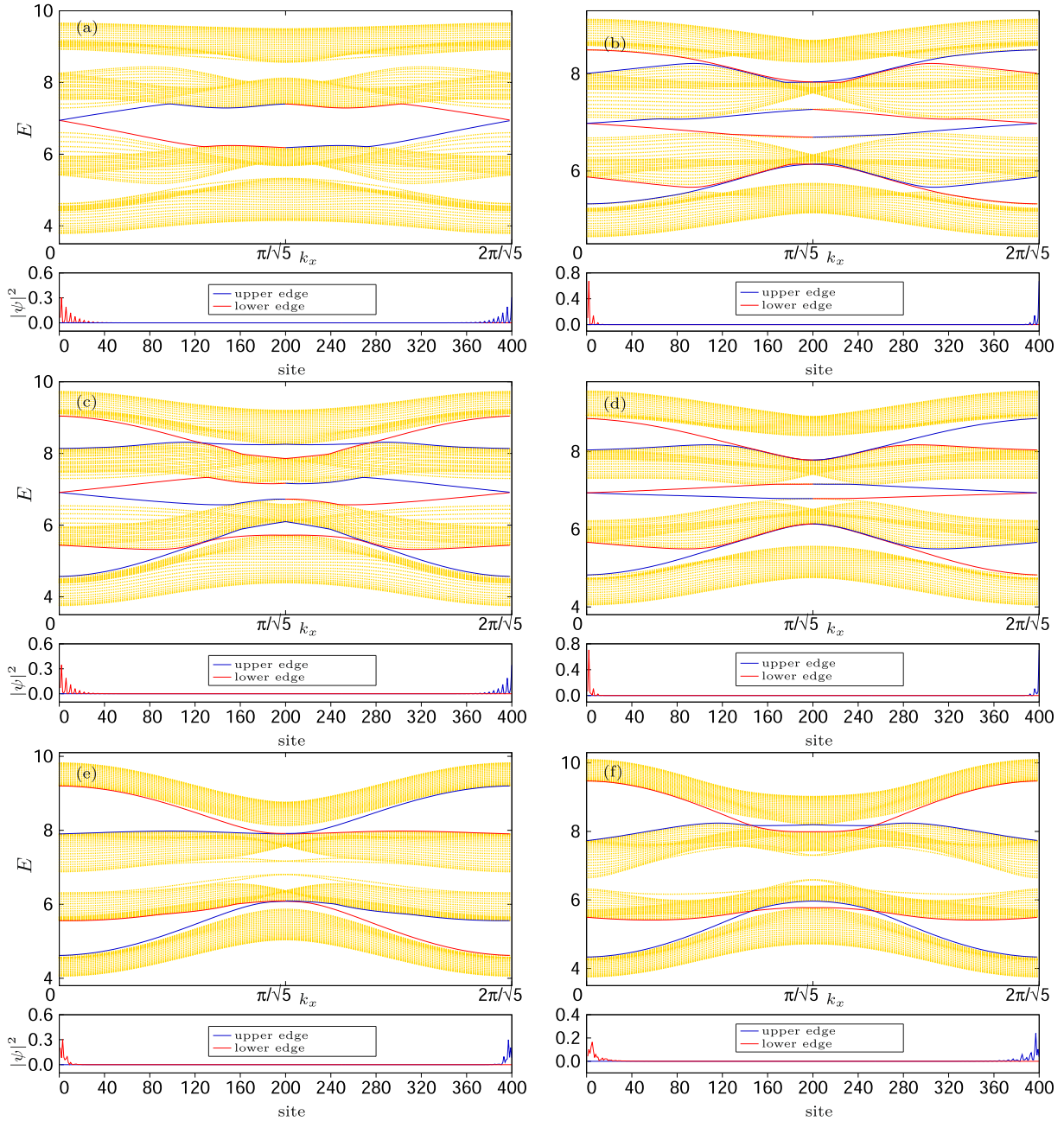


**Fig. 10.** Magnon dispersions of bulk-edge states in the one-dimensional BZ. Upper and lower edge modes are drawn in blue and red lines, respectively, while bulk modes are in golden points. The lower panel indicates variation of probability density of both edge modes with respect to site number for a fixed  $k_x$ . Values of the parameters are: (a)  $K_x = -0.8, K_y = -0.6, K'_x = -1, K'_y = 0.4$  for  $\ell = (01\bar{1}0)$ , (b)  $K_x = -0.7, K_y = -0.2, K'_x = -0.5, K'_y = 0.1$  for  $\ell = (100\bar{1})$ , (c)  $K_x = -0.8, K'_x = -1, K'_y = -0.4$  for  $\ell = (2\bar{3}3\bar{2})$ , (d)  $K_x = -1, K_y = -0.1, K'_x = -0.6, K'_y = -0.3$  for  $\ell = (1\bar{2}2\bar{1})$ , (e)  $K_x = -0.7, K_y = -0.8, K'_x = -0.1, K'_y = -0.5$  for  $\ell = (1\bar{1}1\bar{1})$ , and (f)  $K_x = -0.7, K_y = -0.4, K'_x = -0.8, K'_y = -0.9$  for  $\ell = (2\bar{2}2\bar{2})$ , with  $K_z = -2, K'_z = -1, D_m = 1, h = 1$ . No value is assigned to those parameters when they are zero.

may appear for other combinations of parameter with different values also. But, no additional phase other than those six is by any means found to appear.

Gapless edge states are shown in Fig. 4, where the number of edge states are found to satisfy the ‘bulk-edge correspondence’ rule which states that sum of the Chern number up to the  $i$ -th band,  $\nu_i = \sum_{j \leq i} \mathcal{C}_j$ , is equal to the number of pair of edge states in the gap [25]. Which means that the values of the Chern numbers can be derived, otherwise, from the edge state pattern itself.

Topological phase transition (TPT) may be noted in the parameter space upon changing the values of the parameters. One such transition occurs when  $K'$  becomes non-zero but  $J = -1$  and  $D_m = 0.5$ . In this case,

the system undergoes a transition from the state  $(11\bar{1}\bar{1})$  to another state  $(11\bar{2}0)$ . Distribution of  $\mathcal{C}$ s of those two phases around the transition point can be understood in the following way. Gap between the upper two bands vanishes at the transition point in the parameter space due to the presence of a Dirac cone at the band touching point. When the gap reopens  $\mathcal{C}$ s of the respective upper two bands change by  $\pm 1$ , resulting in the redistribution of them. Occurrence of other TPTs may be explained in similar fashion. For example, transition from  $(11\bar{1}\bar{1})$  to  $(1\bar{1}1\bar{1})$  takes place by switching on the  $K$ . In this case, two intermediate bands touch in such a way that a Dirac cone is formed at the band touching point.

Another pair of TPT is shown in Fig. 5, where the appearance of topological phases is noted with the variation of  $K'$ . The energies,  $E_1, E_2$ ,

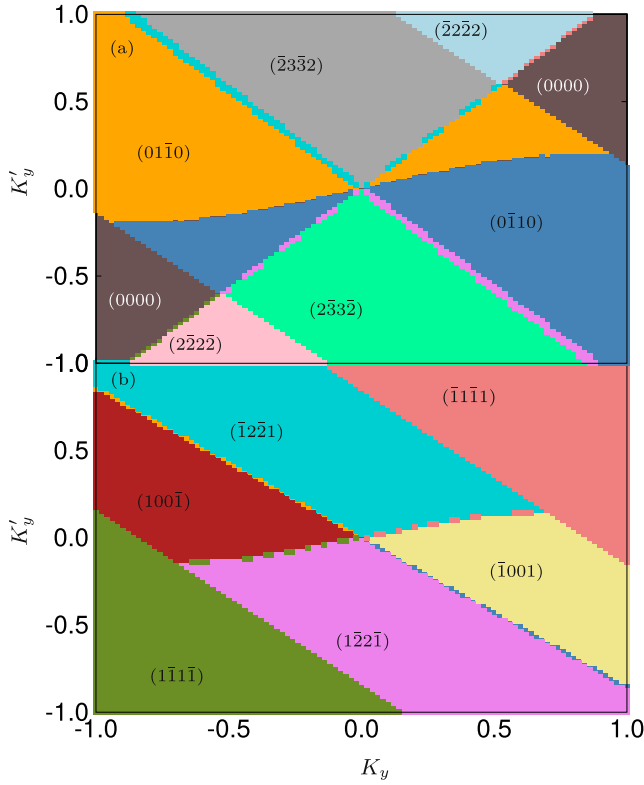


**Fig. 11.** Regions of TMI phases of the system in  $K_y$ - $K'_y$  parameter space for (a)  $K'_x = -0.8$ , and (b)  $K'_x = -0.6$ , with  $K_x = -0.7, K_z = -2, K'_z = -1, D_m = 1, h = 1$ . Trivial region is indicated by (0000).

$E_3$  and  $E_4$  are denoted according to the ascending order of their values. Fig. 5 (a) shows that two nontrivial topological phases,  $(1\bar{1}\bar{1}\bar{1})$  and  $(002\bar{2})$  appear around  $K'_y = -0.5$ . TMI with  $(1\bar{1}\bar{1}\bar{1})$  is found when  $K'_y < -0.16$ , as shown in Fig. 5 (b). Upon increase of  $K'_y$ , Chern numbers of the lower two bands remain unchanged while those of upper two bands are exchanged by  $\pm 1$  leading to a new topological phase with  $(11\bar{2}0)$ . Transition between the same set of topological phases may take place in a variety of ways. Variation of  $\kappa_{xy}$  with respect to  $K'_y$  for four different TMI phases is shown in Fig. 6 with different colors. Those are plotted when  $k_B T = 20$ . Sudden jump in  $\kappa_{xy}$  corresponds to the point where TPT occurs. Similarly, variation of  $\kappa_{xy}$  with respect to  $T$  is shown in Fig. 7.

### 3.2. Anisotropic Kitaev coupling

Anisotropic Kitaev coupling corresponds to  $K_x \neq K_y \neq K_z$  as well as  $K'_x \neq K'_y \neq K'_z$ . Additional conditions,  $J = 0$  and  $J' = 0$ , are assumed to make the system closer to the Kitaev model. In this limit, system only holds the Kitaev terms apart from the DMI. Kitaev model with anisotropic NN coupling, ( $K_x \neq K_y \neq K_z$ ), on both the honeycomb and CaVO lattices have been solved exactly [10,19]. Both the systems host gapless and gapped phases in the ground state phase diagram. Identically, both the systems exhibit a unique topological phase,  $\mathcal{C} = (1\bar{1})$ , in the presence of magnetic field, when they are studied in terms of Majorana fermion.

However, in this study, a dozen of TMI phases is found in the presence of anisotropic Kitaev couplings on the NN and NNN bonds together with NNN DMI and external magnetic field. Band structures for six different TMI phases, are shown in Fig. 8. Dispersion relations along the paths in BZ are shown in Fig. 9, for six different cases. Dispersions of bulk-edge states in the one-dimensional BZ have been shown in Fig. 10. A comprehensive topological phase diagram of the system for the anisotropic case is shown in Fig. 11. Variation of  $\kappa_{xy}$  with respect to  $K_y$  and  $K'_y$  for different TMI phases is shown in Fig. 12. Those are plotted for

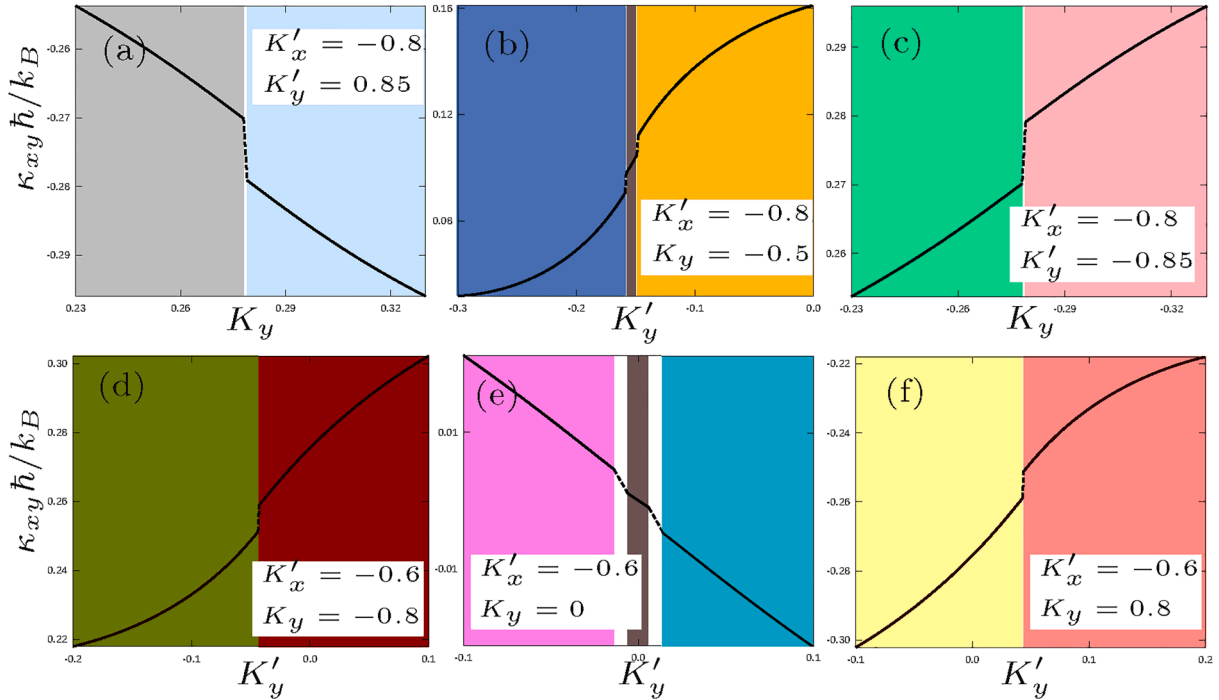


**Fig. 12.** Variation of  $\kappa_{xy} \hbar / k_B$  in the parameter space when  $K_x = -0.7, K_z = -2, K'_z = -1, D_m = 1, h = 1, k_B T = 20$ . Different regions are identified with distinct colors, those are used before in Fig. 11.

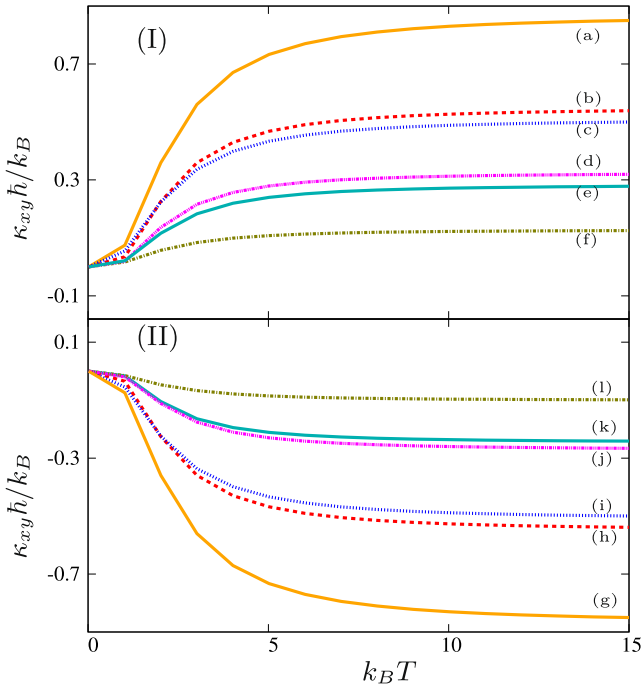


**Fig. 13.** (I) Variation of  $\kappa_{xy}(T)$  with  $T$  for (a)  $K_x = -0.8, K_y = -0.6, K'_x = -1, K'_y = 0.4$  for  $\mathcal{C} = (01\bar{1}0)$ , (b)  $K_x = -0.7, K_y = -0.2, K'_x = -0.5, K'_y = 0.1$  for  $\mathcal{C} = (100\bar{1})$ , (c)  $K_x = -0.8, K'_x = -1, K'_y = -0.4$  for  $\mathcal{C} = (2\bar{3}3\bar{2})$ , (d)  $K_x = -1, K_y = -0.1, K'_x = -0.6, K'_y = -0.3$  for  $\mathcal{C} = (1\bar{2}2\bar{1})$ , (e)  $K_x = -0.7, K_y = -0.8, K'_x = -0.1, K'_y = -0.5$  for  $\mathcal{C} = (1\bar{1}1\bar{1})$ , and (f)  $K_x = -0.7, K_y = -0.4, K'_x = -0.8, K'_y = -0.9$  for  $\mathcal{C} = (2\bar{2}2\bar{2})$ , with  $K_z = -2, K'_z = -1, D_m = 1, h = 1$ . (II) Variation of  $\kappa_{xy}(T)$  for the conjugate phases. No value is assigned to those parameters when they are zero.

$k_B T = 20$ . Similarly, variation of  $\kappa_{xy}$  with respect to  $T$  is shown in Fig. 13. All the figures are drawn for fixed values of the parameters,  $K_z = -2, K'_z = -1, D_m = 1$  and  $h = 1$ .

The remaining six TMI phases are defined by simultaneously reversing the sign of  $\mathcal{C}$  for all four bands, which are henceforth termed as the conjugate phases. Those conjugate phases are obtained by reversing the sign of either  $K'_y$  alone or that of both  $K_y$  and  $K'_y$  simultaneously in the parameter space, but, without changing the signs and values of remaining other parameters. The specific values of  $K_y$  and  $K'_y$ , in addition, will determine which criterion will be obeyed for the emergence of a particular conjugate phase. However, no figure corresponding to those conjugate phases is shown in this article.

The band structure for TMI phase having  $\mathcal{C} = (01\bar{1}0)$  is shown in Fig. 10 (a), which is obtained for  $K_x = -0.8, K_y = -0.6, K'_x = -1$  and  $K'_y = 0.4$ . The conjugate TMI phase with  $\mathcal{C} = (0\bar{1}10)$  appears if the value of  $K'_y$  is changed to  $-0.4$ . System exhibits another TMI phase with  $\mathcal{C} = (2\bar{3}3\bar{2})$  when NN Kitaev interactions along the  $y$  bond is made zero, ( $K_y = 0$ ), keeping other parameters unchanged. The corresponding band structure is shown in Fig. 10 (c). The conjugate TMI with  $\mathcal{C} = (2332)$  is found just reversing the sign of  $K'_y$ . TMI phase with  $\mathcal{C} = (100\bar{1})$  emerges when  $K_x = -0.7, K_y = -0.2, K'_x = -0.5$  and  $K'_y = 0.1$ , which is shown in Fig. 10 (b). But the conjugate TMI phase with  $\mathcal{C} = (\bar{1}001)$  appears in this case if both  $K_y$  and  $K'_y$  reverse their sign. The band structure of the system obtained for  $K_x = -1, K_y = -0.1, K'_x = -0.6$  and  $K'_y = -0.3$ , is shown in Fig. 10 (d). This corresponds to the topological phase having  $\mathcal{C} = (1\bar{2}2\bar{1})$ . Conjugate of this TMI phase appears if  $K'_y$  picks up the reverse sign. At  $K_x = -0.7, K_y = -0.8, K'_x = -0.1$ , TMI phase with  $\mathcal{C} = (1\bar{1}1\bar{1})$  and its conjugate  $\mathcal{C} = (\bar{1}111)$  appear for  $K'_y = -0.5$ , and  $K'_y =$

0.5, respectively. The former is shown in Fig. 10 (e). Finally, Fig. 10 (f) corresponds to the band structure of another TMI phase with  $\mathcal{C} = (2\bar{2}2\bar{2})$ . The corresponding conjugate TMI phase,  $\mathcal{C} = (2222)$ , appears when signs of both  $K_y$  and  $K'_y$  are reversed. The TMI phase,  $\mathcal{C} = (1\bar{1}1\bar{1})$ , is found to appear in both the cases of isotropic and anisotropic Kitaev couplings. However, no conjugate phase is found in the isotropic case.

A comprehensive topological phase diagram of the system for the anisotropic case is shown in Fig. 11 for  $K_x = -0.7$ . Two diagrams (a) and (b) are drawn by varying  $K_y$  and  $K'_y$ , respectively, where the value of  $K'_x$  remains fixed at  $-0.8$  and  $-0.6$  in the respective cases. Trivial regions are indicated by (0000), where all the  $\mathcal{C}$ s are zero.

Variation of  $\kappa_{xy}h/k_B$  in the parameter space is shown in Fig. 12 when  $K_x = -0.7, K_z = -2, K'_z = -1, D_m = 1, h = 1$ , and  $k_B T = 20$ . Here, different regions are identified with distinct colors, those are used before in Fig. 11. Sudden jump in  $\kappa_{xy}$  is noted where TPT takes place. Variation of  $\kappa_{xy}$  with respect to  $T$  for six different TMI phases along with their conjugate phases is shown in Fig. 13, with different colors. Signs of  $\kappa_{xy}$  for a particular TMI phase and its conjugate are of opposite to each other. This corresponds to the fact that signs of the  $\mathcal{C}$ s of a definite phase are opposite to those of the corresponding conjugate phase. Thus,  $\kappa_{xy}$  for all the twelve distinct topological phases have been shown in this figure.

#### 4. Discussion

Topological properties based on the bosonic magnon excitation of the FM Kitaev-Heisenberg model on CaVO lattice in the presence of DMI have been investigated extensively in this study. The model comprises of Heisenberg and Kitaev terms both on NN and NNN bonds. Both isotropic as well as anisotropic couplings are considered. A sizable number of TMI phase appears upon variation of parameter values. Topological phases have been characterized in terms of Chern numbers which are evaluated numerically. DMI on a particular combination of NNN bonds is found crucial for the emergence of the TMIs. On the other hand, NN DMI has no role for the same.

It has been indicated in the previous studies that FM Kitaev model with NN anisotropic couplings exhibits a unique topological phase based on the Majorana fermion representation both for the honeycomb and CaVO lattices in the presence of magnetic field [10,19]. Interestingly, the situation is different in case of FM Kitaev-Heisenberg system, however, when solved in terms of bosonic magnon excitations. The present investigation reveals that multiple topological phases arise in Kitaev-Heisenberg model on CaVO lattice when both NN and NNN terms are there. No topological phase is there for NN term alone. In addition, topological properties of the Kitaev-Heisenberg model on the honeycomb lattice are drastically different from those of CaVO lattice perhaps because of their different symmetries.

In case of honeycomb lattice, nontriviality in the two-band Kitaev-Heisenberg system is induced by the presence of SAI term,  $\Gamma(S_i^a S_j^b + S_i^b S_j^a)$  [12]. Conjugate topological phases appear upon sign reversal of  $\Gamma$ , the strength of SAI. But no role of DMI is found there. On the other hand, no effect of SAI term is found on the topological properties of four-band Kitaev-Heisenberg system for CaVO lattice, where, NNN DMI term is found indispensable. Conjugate phases appear when the signs of Kitaev terms,  $K_y$  and  $K'_y$  are reversed depending on the situation. No conjugate phase appears in the fermionic Kitaev models.

NNN Kitaev and Heisenberg terms could not lead to new topological phase for the honeycomb lattice [12]. But a number of new topological phases emerge as soon as the third neighbor Kitaev and Heisenberg terms are introduced. On the other hand, the system hosts multiple topological phases in the presence of NNN Kitaev and Heisenberg terms, in case of CaVO lattice. It is expected that numerous novel topological phases with higher values of Chern numbers will come up if third neighbor Kitaev and Heisenberg terms are taken into account.

Therefore, the topological properties of FM Kitaev-Heisenberg models on both CaVO and honeycomb lattices are different when studied in terms of bosonic magnon excitations in comparison to the exactly solvable FM Kitaev models on the same lattices based on the Majorana representation.

#### CRediT authorship contribution statement

**Moumita Deb:** Conceptualization. **Asim Kumar Ghosh:** Conceptualization.

#### Declaration of Competing Interest

The authors declare that they have no known competing financial interests or personal relationships that could have appeared to influence the work reported in this paper.

#### Acknowledgments

MD acknowledges the UGC fellowship, No. 524067 (2014), India.

#### References

- [1] D.J. Thouless, M. Kohmoto, P. Nightingale, M. den Nijs, *Phys. Rev. Lett.* 49 (1982) 405.
- [2] Y. Hatsugai, *Phys. Rev. Lett.* 71 (1993) 3697.
- [3] Y. Onose, T. Ideue, H. Katsura, Y. Shiomi, N. Nagaosa, Y. Tokura, *Science* 329 (2010) 297.
- [4] H. Katsura, N. Nagaosa, P.A. Lee, *Phys. Rev. Lett.* 104 (2010), 066403.
- [5] I. Dzyaloshinskii, *J. Phys. Chem. Solids* 4 (1958) 241.
- [6] T. Moriya, *Phys. Rev.* 120 (1960) 91.
- [7] L. Zhang, J. Ren, J.-S. Wang, B. Li, *Phys. Rev. B* 87 (2013), 144101.
- [8] R. Seshadri, D. Sen, *Phys. Rev. B* 97 (2018), 134411.
- [9] R. Chisnell, et al., *Phys. Rev. Lett.* 115 (2015), 147201.
- [10] A. Kitaev, *Ann. Phys.* 321 (2006) 2.
- [11] D.G. Joshi, *Phys. Rev. B* 98 (2018) 060405(R).
- [12] M. Deb, A.K. Ghosh, *J. Phys.: Condens. Matter* 31 (2019), 345601.
- [13] M. Deb, A.K. Ghosh, *J. Phys.: Condens. Matter* 32 (2020), 365601.
- [14] A. Sil, A.K. Ghosh, *J. Phys.: Condens. Matter* 31 (2019), 245601.
- [15] S.A. Owerre, *J. Phys.: Condens. Matter* 30 (2018) 28LT01.
- [16] M. Deb, A.K. Ghosh, *Eur. Phys. J. B* 93 (2020) 145.
- [17] S. Taniguchi, et al., *J. Phys. Soc. Jpn.* 64 (1995) 2758.
- [18] I. Bose, A. Ghosh, *Phys. Rev. B* 56 (1997) 3149.
- [19] S. Yang, D.L. Zhou, C.P. Sun, *Phys. Rev. B* 76 (2007) 180404(R).
- [20] T. Fukui, Y. Hatsugai, H. Suzuki, *J. Phys. Soc. Jpn.* 74 (2005) 1674.
- [21] F.C. Alcaraz, W.F. Wreszinski, *J. Stat. Phys.* 58 (1990) 45.
- [22] D.N. Aristov, S.V. Maleyev, *Phys. Rev. B* 62 (2000) R751.
- [23] R. Matsumoto, S. Murakami, *Phys. Rev. Lett.* 106 (2011), 197202.
- [24] R. Matsumoto, S. Murakami, *Phys. Rev. B* 84 (2011), 184406.
- [25] A. Mook, J. Henk, I. Mertig, *Phys. Rev. B* 90 (2014), 024412.